Robust Interpenetrating Network type Amphoteric Ion Exchange Membrane for high performance Vanadium Redox Flow Batteries

Pratyush Patnaik[a,b,#], Prashant Kumar,[a,b,#], Ritika Sharma[a,b], Pankaj D. Indurkar[a,b], Vinod K. Shahi[a,b,c]*, Uma Chatterjee[a,b]** , Vaibhav Kulshrestha[a,b]***

[a]*CSIR-Central Salt and Marine Chemicals Research Institute, Gijubhai Badheka Marg, Bhavnagar, 364 002, Gujarat, India*
[b]*Academy of Scientific and Innovative Research (AcSIR), Ghaziabad-201002, India*
[c]*Department of Polymer and Process Engineering, Indian Institute of Technology Roorkee, Saharanpur Campus, Saharanpur-247001(UP) India*
E-mail: *vinodkshahi@gmail.com; **dr.umachatterjee@gmail.com, umac@csmcri.res.in; *** vaibhavk@csmcri.res.in, vaibhavphy@gmail.com

[#] *Contributed equally*

Section S1. Analytical characterizations

Fourier Transform Infrared Spectroscopy coupled with Attenuated Total Reflectance (FTIR-ATR) was used to investigate the chemical structure and identify functional groups in the fully dried samples. Spectral data were collected using a Spectrum GX Series 49387 spectrometer in the range of 4000–400 cm^{-1}. The KBr pellet method was utilized to ensure optimal spectral clarity and resolution.

X-ray Photoelectron Spectroscopy (XPS) was conducted using a Thermo Scientific Nexsa G2 surface analysis system to investigate the elemental composition, chemical states, and surface functionalities of the samples. This technique enabled detailed analysis of the surface chemistry, providing insights into the bonding environments and atomic-level interactions within the membrane materials.

The thermal stability of the AMIPM-x membranes was evaluated using a Thermogravimetric Analyzer (NETZSCH TG 209F1 Libra, TGA209F1D-0105-L) under a nitrogen atmosphere, with a heating rate of 10 °C/min over a temperature range of 30 to 800 °C.

The mechanical properties of the membrane samples, including stress and elongation at break, were evaluated using a Zwick Roell Z2.5 universal testing machine following the ISO 527 S2 standard. Specimens measuring 2.5 cm in length, 0.35 cm in width, and 0.18 mm in thickness were tested at a crosshead speed of 20 mm/min. Data acquisition and analysis were performed using testXpert II V3.5 software.

Scanning Electron Microscopy (SEM) analysis was performed after applying gold sputter coating to the bead samples under a pressure range of 0.1–1.0 Pa. Micrographs were acquired using a LEO microscope at a chamber pressure of 10-3 to 10-2 Pa, with an accelerating voltage (EHT) of 15.00 kV and a collector bias of 300 V. Energy-dispersive X-ray spectroscopy (EDX) and elemental mapping of the AMIPM-x membrane were conducted using a LEO VP1430 system.

X-ray Photoelectron Spectroscopy (XPS) was conducted using a Thermo Scientific Nexsa G2 surface analysis system to investigate the elemental composition, chemical states, and surface functionalities of the samples. This technique enabled detailed analysis of the surface chemistry, providing insights into the bonding environments and atomic-level interactions within the membrane materials.

X-ray diffraction (XRD) patterns were obtained using a Philips X'Pert diffractometer equipped with Cu Kα radiation (λ = 1.54056 Å).

Atomic force microscopy (AFM) studies of dried membranes (AMIPM-x) samples were performed at 30 °C using NTEGRA AURA (NTMDT) instrument in semi-contact mode SPM S-2 NSG 01tip with approx. 10 nm radius of curvature (natural frequency for the cantilever was 300 kHz).

Section S2. Procedures for determining water uptake, swelling ratio, ion-exchange capacity, ionic conductivity (κ^m), and vanadium ion (VO^{2+}) permeability of the anion exchange (IPAEM-120), amphoteric (AMIPM-x), and proton exchange (IPPEM-126) membranes.

The membrane was equilibrated in the DI water at room temperature for 24 hrs. The excess water on the surface of the wet membrane was removed by tissue paper and the weight of wet membrane (W_{wet}) was determined. The wet sample was dried in vacuum oven at 80 °C and constant dry weight (W_{dry}) was recorded for the estimation of water uptake (WU):-

$$WU\ (\%) = \frac{W_{wet} - W_{dry}}{W_{dry}} \times 100 \quad \text{(S1)}$$

The swelling ratio (SR) of the membrane zwitterionic membranes was measured by immersing the membrane in water at 60 °C for 12 hrs using the given equation; where L_{wet} and L_{dry} are the lengths of the wet and dry membranes:-

$$SR\ (\%) = \frac{L_{wet} - L_{dry}}{L_{dry}} \times 100 \quad \text{(S2)}$$

Ion exchange capacity (IEC_{SO_3H}) of amphoteric (AMIPM-x) and proton exchange membrane (IPPEM-126) samples was estimated by the acid base titration by following equation:-

$$IEC = \frac{V_{NaOH} \times C_{NaOH}}{W_{dry}} \quad \text{(S3)}$$

Where *C* and *V* denote the concentration and volume of HCl. The measuring error of IEC is ±0.01 meq/g

IEC_{NR3+} of the amphoteric anion exchange (IPAEM-120) and amphoteric (AMIPM-x) membranes was measured by Mohr's titration method. Accurately weighted dry membranes were kept in 1M NaCl solution for 24 h then excessive NaCl was washed off by DI water. After that, the membranes were put into 0.5 M KNO_3 solution to exchange the Cl^- with NO_3^-. The amount of exchange Cl^- was titrated with 0.01 M $AgNO_3$ solution using a potassium chromate indicator.

$$IEC = \frac{C_{AgNO_3} V_{AgNO_3}}{W_{dry}} \tag{S4}$$

The ionic conductivity of amphoteric AMIPM-x membranes was measured in DI water using four-electrode AC impedance potentiostat/galvanostat frequency response analyser (Eco Chemie, B.V. Utrecht, The Netherlands Auto Lab, model PGSTAT 302N) over 1-10^6 Hz frequency range. The membrane was sandwiched between two in-house made up of stainless steel circular electrodes (1.0 cm^2). Direct current (DC) and sinusoidal alternating currents (AC) were supplied to the respective electrodes for recording the frequency at 1 μA/s scanning rate. The membrane resistance was determined from the Nyquist plots using Fit and Simulation method. Membrane resistance (R^m) was measured in equilibration with deionized water and membrane conductivity (κ^m) was estimated by the following equation, Where L and A are the membrane thickness and membrane conducting area respectively.

$$\kappa^m\,(S/cm) = \frac{L\,(cm)}{\left[R^m\,(\Omega) \times A\,(cm^2)\right]} \tag{S5}$$

Hydration number (λ) is defined as the average number of water molecules per ionic group. This reflects the local molecular-scale hydration structure in the hydrophilic transport site, regardless of the membrane dimension, constituents, and macroscale/microscale phase-separation structures. Contrary to WU, λ principally should provide an insight into microscopic change and how local intermolecular (water–ion–polymer) interactions affect ion transport in the membrane. In the current research state, the λ value is generally estimated from WUs by equation 6.

$$\lambda = \frac{WU \times 10}{18 \times IEC} \tag{S6}$$

The permeability of vanadium ion (VO^{2+}) across the different membranes was measured in a two-compartment permeability cell separated by a membrane sample (12.56 cm^2). Compartment (A) was filled with $VOSO_4$ (1 M) solution in 3 M H_2SO_4 (35 cm^3), while compartment (B) was filled with $MgSO_4$ (1 M) in 3 M H_2SO_4 (35 cm^3). Both compartments were stirred continuously. $MgSO_4$ was used to neutralize the ionic strengths in both compartments to minimize the osmotic effects. After a certain time interval, a sample of compartment (B) was analyzed for VO^{2+} concentration by ICP analysis. The permeability of the vanadium ion (P, $cm^2\ min^{-1}$) was calculated by the following equation.

$$V_R \frac{dC_R(t)}{dt} = S_A \frac{P}{L}(C_L - C_R(t)) \quad \text{(S7)}$$

Where V_R is the solution volume of the B half-cell, C_L and $C_R(t)$ are the concentrations of vanadium in the A and B cells, S_A and L are the effective area and thickness of the sample membrane, and P is the permeability of VO^{2+}.

$$\text{Ionic Selectivity} = \frac{K^m}{P} \ (\text{S min cm}^{-3}) \quad \text{(S8)}$$

Section S3. VRFB Single cell performance.

The coulombic efficiency (CE), voltage efficiency (VE), and energy efficiency (EE) were determined by the following equations;

$$CE = \frac{\int_0^{t_d} I_d(t)dt}{\int_0^{t_c} I_c(t)dt} \times 100\% \quad \text{(S9)}$$

$$VE = \frac{\int_0^{t_d} U_d(t)dt}{\int_0^{t_c} U_c(t)dt} \times 100\% \quad \text{(S10)}$$

$$EE = CE \times VE = \frac{\int_0^{t_d} U_d(t)dt \,.\, I_d(t)dt}{\int_0^{t_c} U_c(t)dt \,.\, I_c(t)dt} \times 100\%$$

(S11)

Where t_d and t_c represent the discharge and charge durations of the battery, respectively. I_d and I_c correspond to the discharge and charge currents. while U_d and U_c denote the respective discharge and charge voltages.

Section S4. Reaction procedure for the synthesis of the interpolymer proton exchange membrane (IPPEM-126).

IPPEM-126 was synthesized by dissolving predetermined ratios of HDPE and LDPE in xylene inside a batch reactor maintained at 120 °C. Subsequently, styrene and divinylbenzene (DVB) were introduced, and interpolymer free-radical copolymerization was initiated by adding benzoyl peroxide as the radical initiator. The polymerization was allowed to proceed for 6 h at 120 °C. After completion, the resulting copolymer was thoroughly washed with isopropanol and dried in a vacuum oven at 60 °C for 24 h. The dried material was then melt-extruded at approximately 220 °C to produce thin films with an average thickness of ~120 μm. These films were sulfonated using 20% chlorosulfonic acid in 1,2-dichloroethane for 6 h. Prior to electrochemical evaluation, the membranes were equilibrated in 1 M H_2SO_4 to ensure complete protonation.

Section S5. Cost and processability of the prepared membranes compared with PFSA-based membranes

Beyond electrochemical performance, the AMIPM membrane design offers significant advantages in terms of economic feasibility and industrial scalability. Commercial state-of-the-art fluorinated membranes (e.g., Nafion) remain prohibitively expensive for large-scale VRFBs (often >\$500 m^{-2}) due to the complex precursor synthesis. In contrast, hydrocarbon-based membranes typically rely on more economical polymer backbones but are often fabricated via solvent-casting processes that require high-boiling solvents (e.g., NMP, DMSO), which incur additional costs for solvent handling, evaporation, and recovery.

The interpenetrating network strategy presented here circumvents both financial bottlenecks. The base matrix is a commercially extruded polyethylene blend, a globally available commodity plastic costing approximately ~\$1.20 kg^{-1}. Furthermore, the functionalization utilizes standard, low-cost commercial monomers and reagents (p-methylstyrene, divinylbenzene, and trimethylamine) via a solvent-free matrix swelling process. By entirely eliminating the costs associated with custom polymer synthesis, highly toxic precursors, and high-boiling solvent recovery, this IPN method presents a highly scalable and economically viable pathway for next-generation VRFB membranes.

Table S1. Cost estimation for AMIPM-x membrane preparation

Material	*Cost (USD)*
HDPE/LDPE	*~\$1.2 Kg^{-1}*
p-methyl styrene	*~\$3-6 L^{-1}*
DVB	*~\$3-5 L^{-1}*
BPO	*~\$8-12 Kg^{-1}*
Xylene	*~\$1.0-1.5 L^{-1}*
IPA	*~\$1.0-1.5 L^{-1}*
Trimethylamine	*~\$2.0-4.0 L^{-1}*
Chlorosulfonic acid	*~\$3.0-5.0 L^{-1}*
Other miscellaneous cost	*~\$8-12 m^{-2}*
Total production cost of the membrane (*x* m^2)	*~\$30-50 m^{-2}*
Liquid reagents (styrene, DVB, chlorosulfonic acid, solvents) are expressed in \$ L^{-1}, while solid materials are reported in \$ kg^{-1}, based on approximate bulk industrial prices.	

.

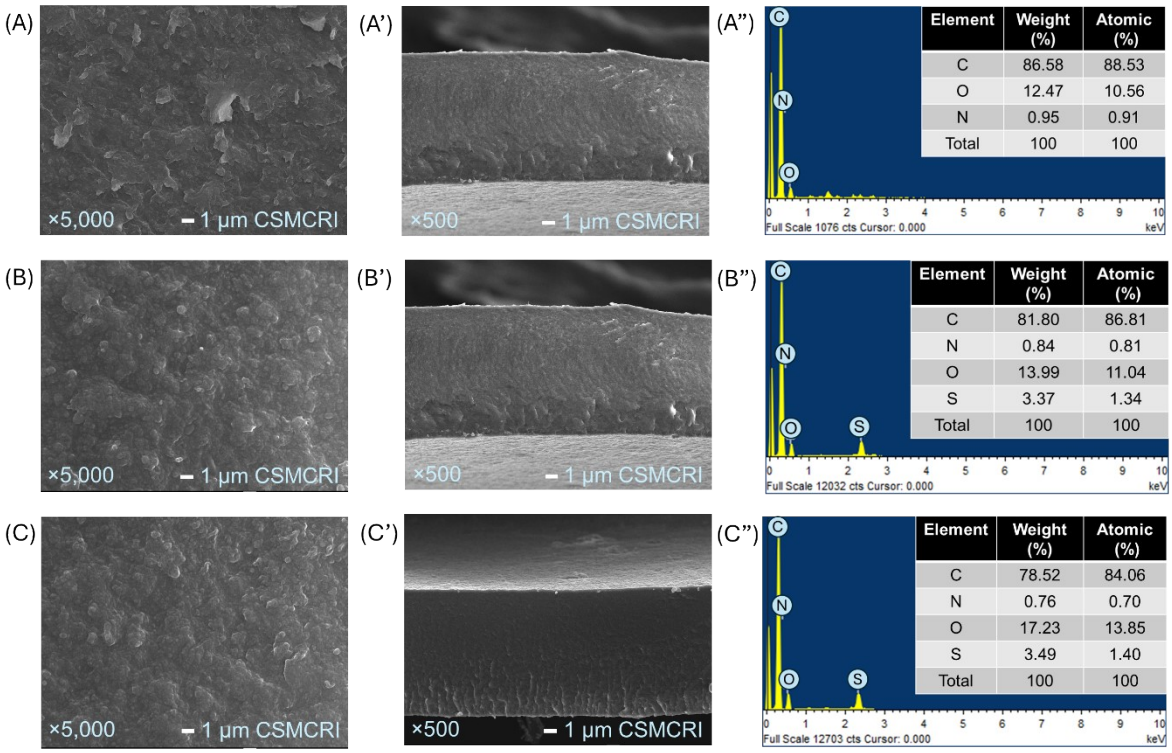

Figure S1. Surface and cross-sectional FE-SEM micrographs along with corresponding EDX spectra of (A, A′, A″) pristine IPAEM-120, (B, B′, B″) AMIPM-122, (C, C′, C″), and AMIPM-124 membranes.

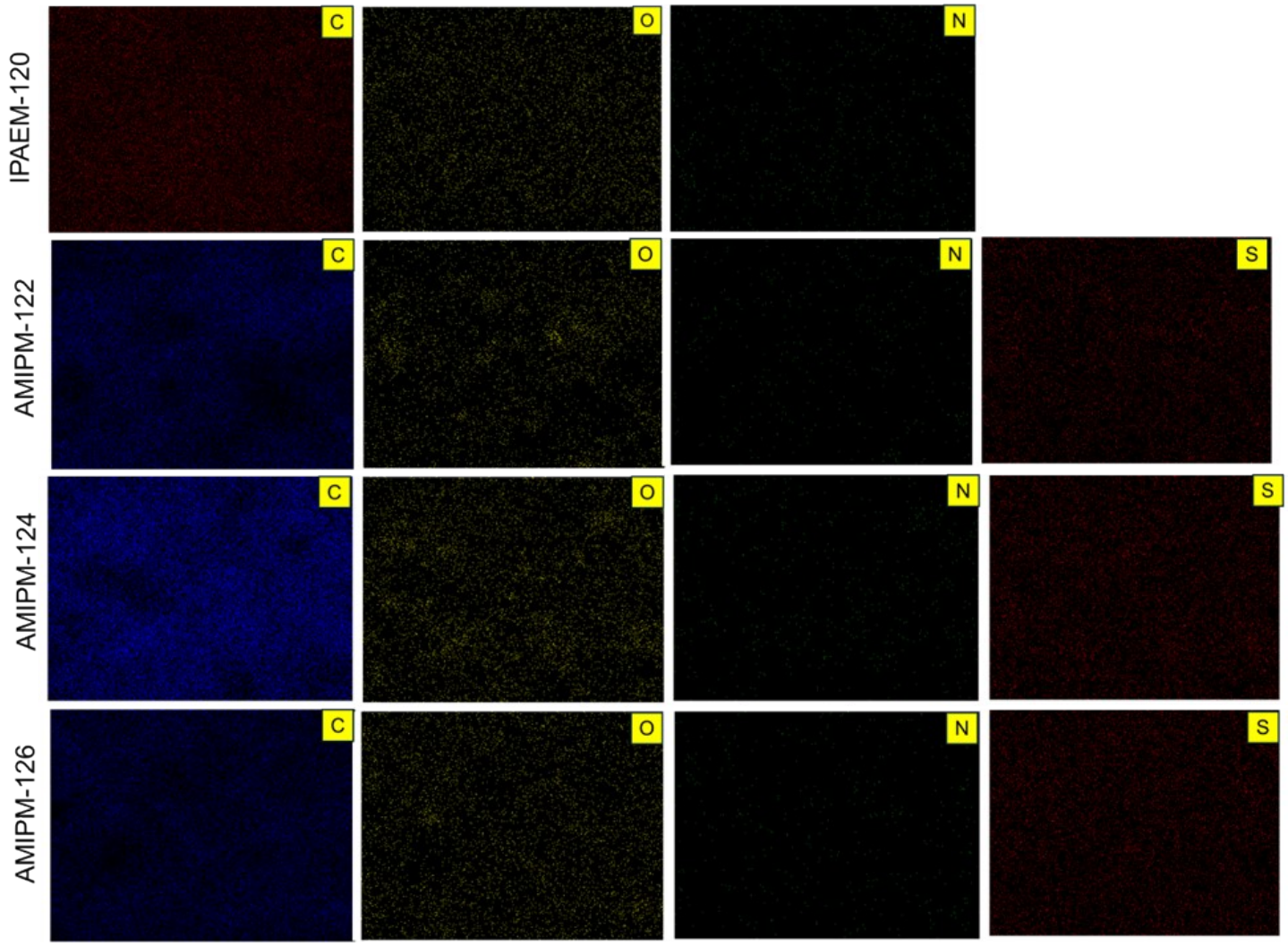

Figure S2. Elemental mapping of different elements presents in the membrane matrix in IPAEM-120, AMIPM-122, AMIPM-124, and AMIPM-126.

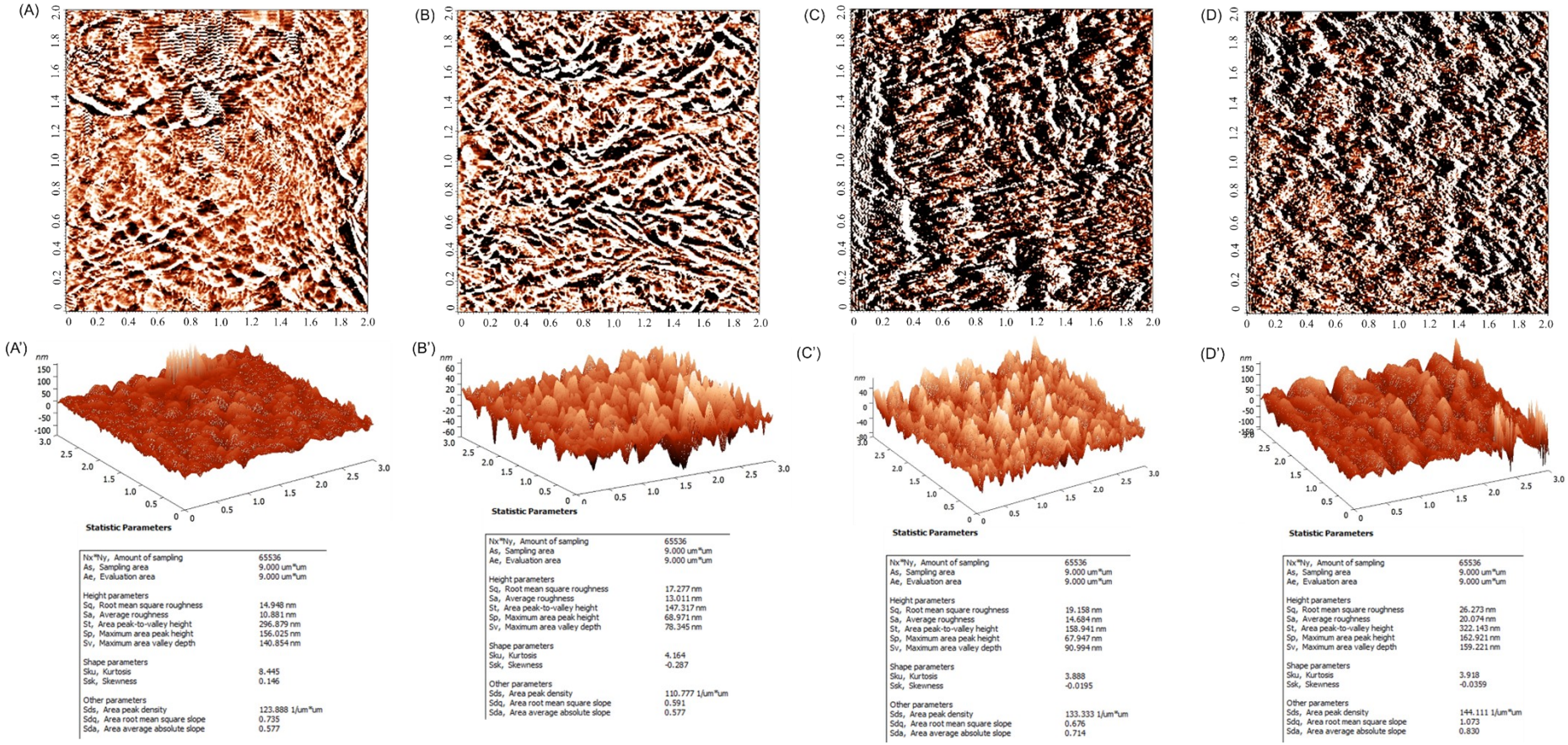

Figure S3. AFM phase images and 3D surface topographies of (A, A') IPAEM-120, (B, B') AMIPM-122, (C, C') AMIPM-124, and (D, D') AMIPM-126 membranes.

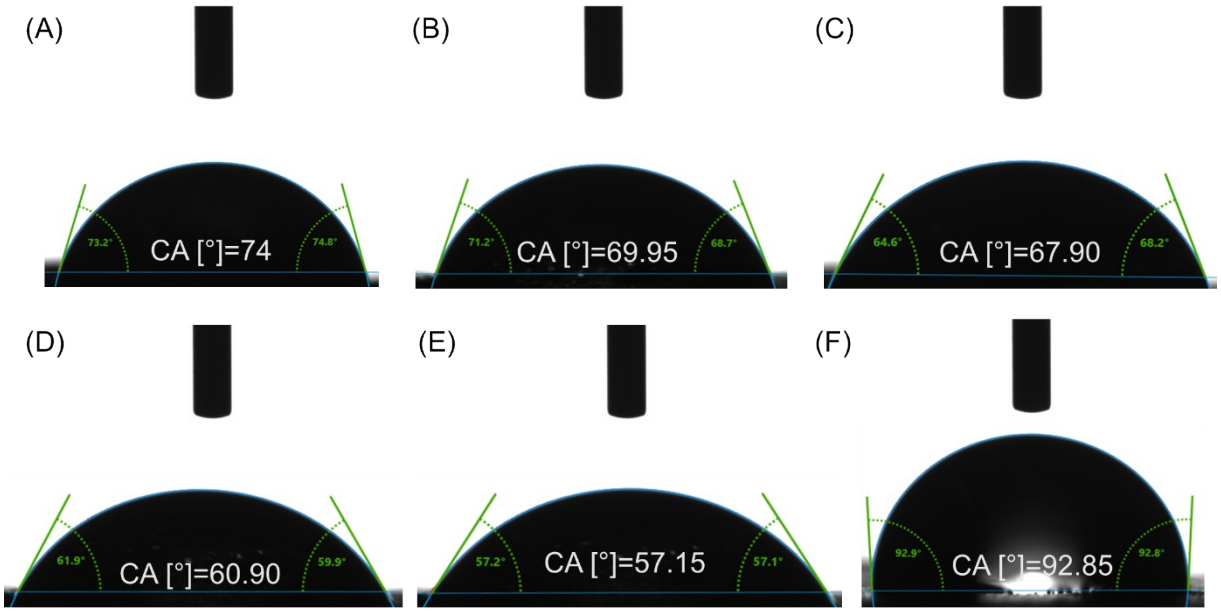

Figure S4. Water contact angle (WCA) images of the membranes: (A) IPAEM-120, (B) AMIPM-122, (C) AMIPM-124, (D) AMIPM-126, (E) IPPEM-126 , and (F) Nafion-117.

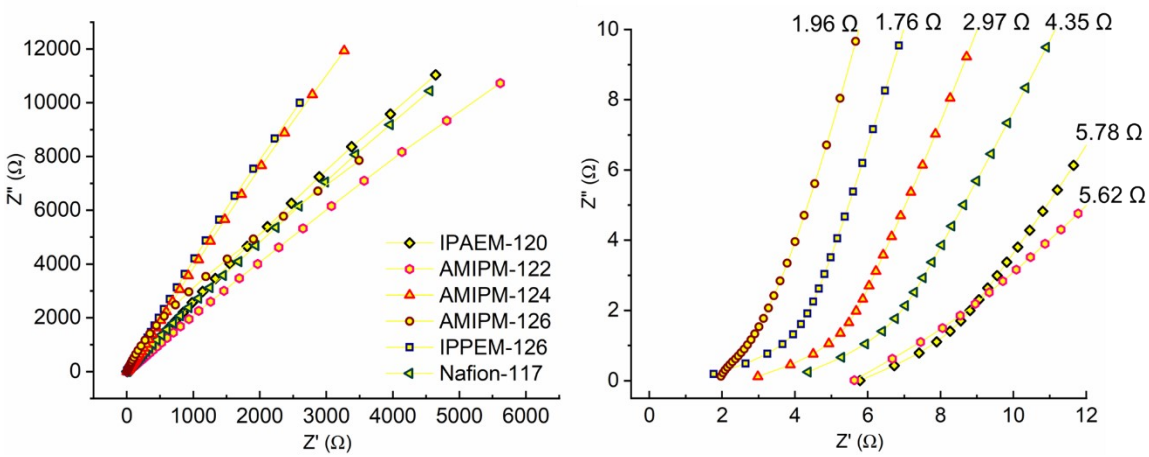

Figure S5. Nyquist plots of the synthesized membranes obtained from electrochemical impedance spectroscopy (EIS). The left graph shows the full impedance profile, while the right graph highlights the low-frequency region used to estimate membrane resistance.

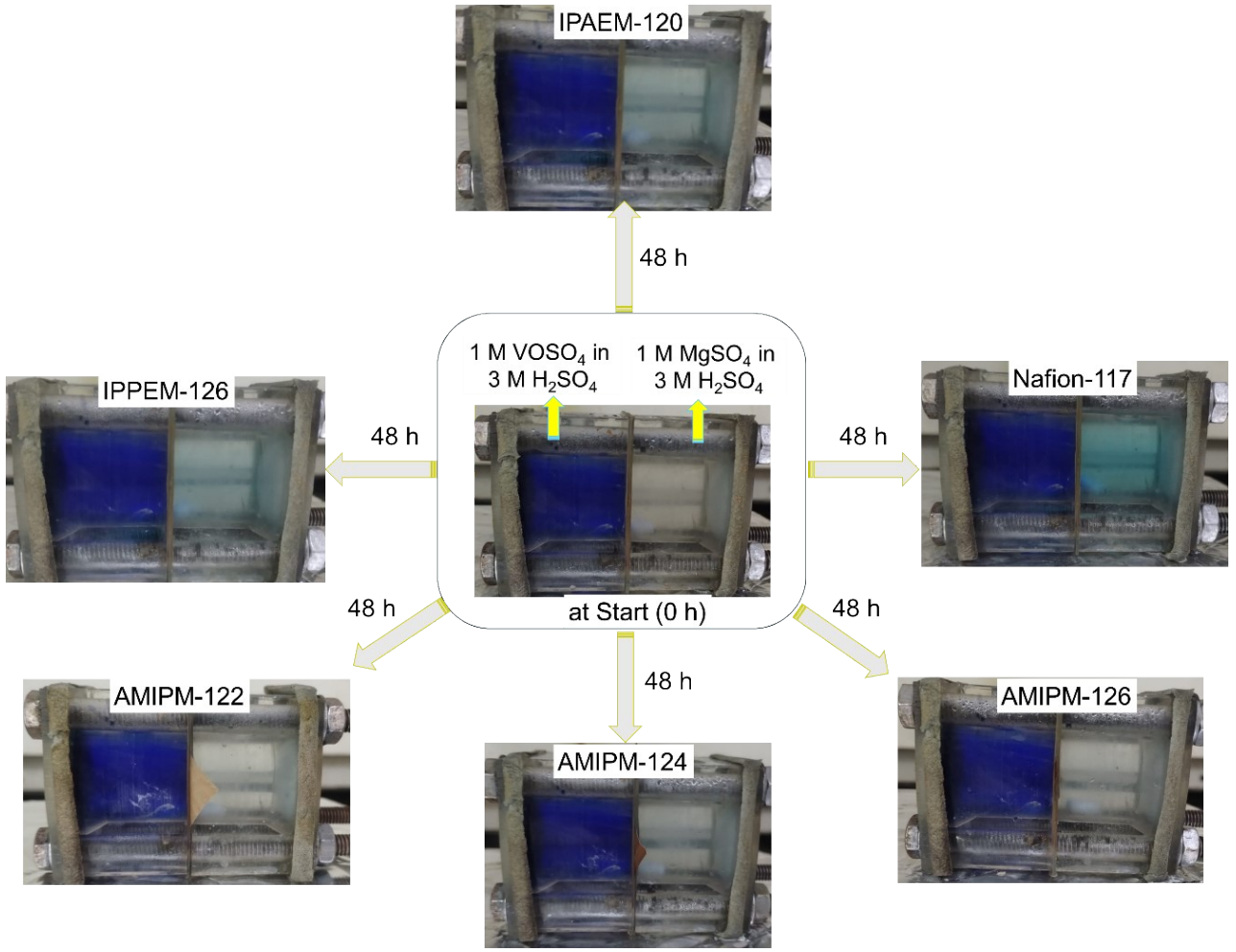

Figure S6. VO^{2+} Vanadium permeability images of the prepared membranes IPAEM-120, AMIPM-122, AMIPM-124, and AMIPM-126 compared with the IPPEM-126 and commercial Nafion-117 membranes.

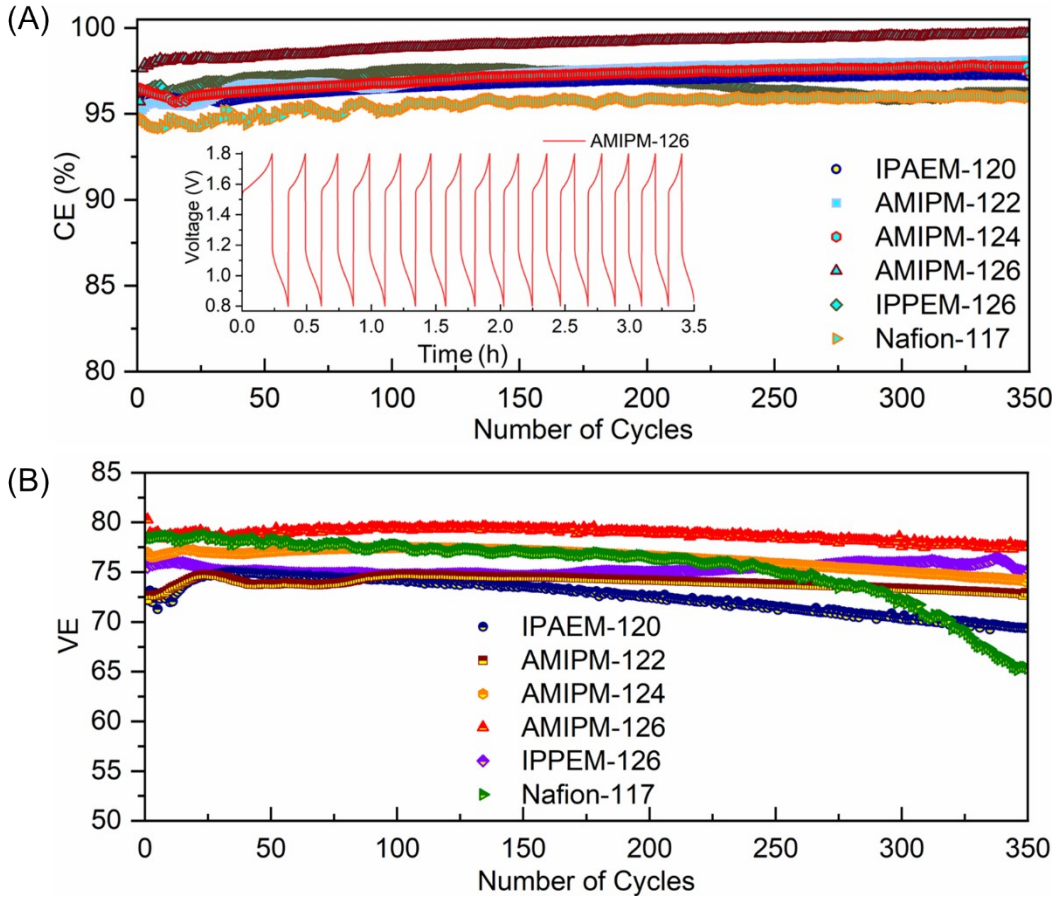

Figure S7. Electrochemical long-term cycling performance of IPAEM-122, AMIPM-122, AMIPM-124, AMIPM-126, and Nafion-117 membranes in a VRFB system at a current density of 130 mA cm^{-2}. (A) Coulombic efficiency (CE) and (B) voltage efficiency (VE).

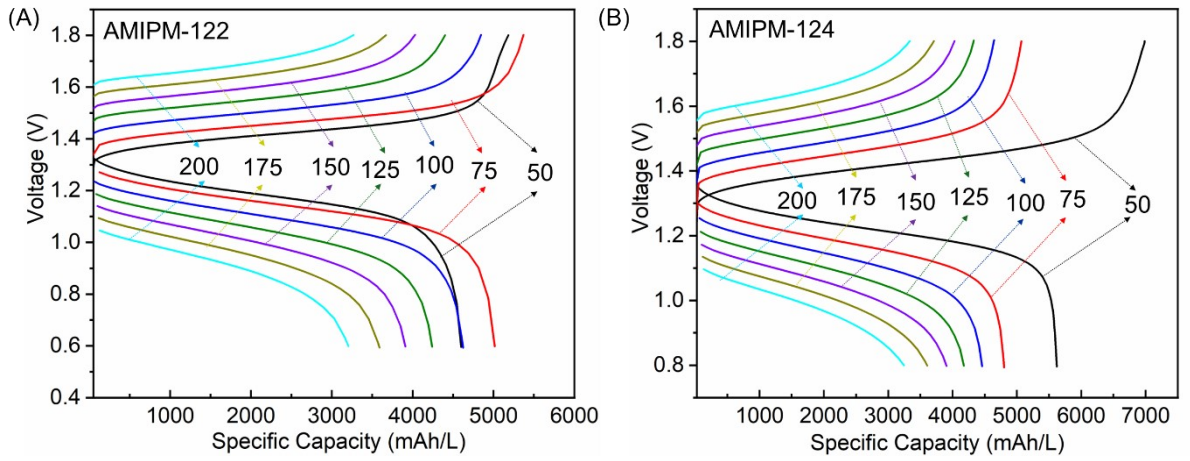

Figure S8. Charge–discharge voltage curves of AMIPM-122 and AMIPM-124 membranes measured at various current densities (50–200 mA cm^{-2}) range.

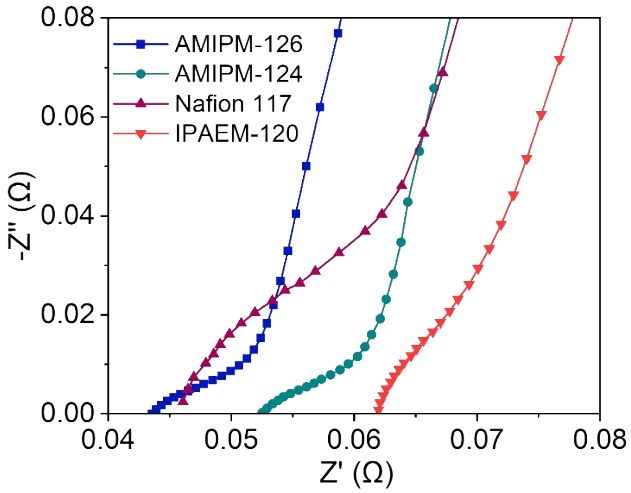

Figure S9. EIS curves of the prepared membranes and Nafion 117 fitted in the VRFB cell with continuous flow of the posolyte and anolyte (1 M V^{n+} + 3 M H_2SO_4).